SCIENTIFIC REPORTS

OPEN

Experimental controlled-NOT gate simulation with thermal light

Tao Peng[1], Vincenzo Tamma[2] & Yanhua Shih[1]

We report a recent experimental simulation of a controlled-NOT gate operation based on polarization correlation measurements of thermal fields in photon-number fluctuations. The interference between pairs of correlated paths at the very heart of these experiments has the potential for the simulation of correlations between a larger number of qubits.

The discovery of the Hanbury Brown and Twiss (HBT) effect[1,2] in 1956 triggered the development of the field of quantum optics. Indeed, this phenomenon motivated numerous studies of multiphoton entanglement and interference not only from a fundamental point of view[3–8] but also toward applications in information processing[9–13], metrology[14,15] and imaging[16–18].

Recent efforts have been made to simulate quantum entanglement using classical light[8,19–24]. These studies are important toward achieving a deeper understanding of the differences between classical and quantum systems. Moreover, although such schemes may suffer of an exponential scaling in the number of resources comparing with the quantum systems[25–27], they make it possible to simulate small-scale quantum systems with simple interferometers without being affected by decoherence. We have recently developed a novel detection scheme that measures the photon-number fluctuation correlation(PNFC) of thermal light[28]. This scheme has been applied to the study of the multi-photon coherence of thermal states[8,23,24,28–30], leading to effects similar to the nonlocal interference characterizing entangled states.

Motivated by these results, we experimentally demonstrate here how multiphoton interference of pairs of correlated optical paths emerges from the measurement of photon-number fluctuations of thermal fields. This phenomenon is not only interesting from a fundamental point of view but also opens the way to the simulation of quantum gate operations. In particular, by using only a pseudo-thermal source[31,32] and a linear optical interferometer, a controlled-NOT (CNOT) gate operation[33–38] is experimentally simulated. The experimental setup (Fig. 1) is a realization in the spatial domain[24] of the theoretical proposal of Tamma and Seiler[8]. In particular, we demonstrate how correlation measurements in the fluctuations of the number of photons at the output of the interferometer not only simulate (Fig. 2) the truth-table of a CNOT-gate (Table 1) but also the Bell correlations (Fig. 3) typical of a CNOT-gate operation.

Results

Description of the experiments.
We describe the experimental setup, depicted schematically in Fig. 1. The light source is a standard pseudo-thermal source consisting of a circularly polarized 633 nm CW laser beam and a rotating ground glass (GG). The diameter of the laser beam is ~2 mm. The size of the tiny diffusers on the GG is roughly a few micrometers. A large number of circularly polarized incoherent wavepackets, or subfields, are scattered from a large number of diffusers. The second-order coherence time of the source is measured to be ~90 ms. The randomly scattered wavepackets are then split by a non-polarizing beamsplitter into two beams, the "control beam" c and the "target beam" t. A polarizer P_i and a half-wave plate HWP$_i$ prepare each beam $i = c, t$ at an arbitrary polarization direction $\vec{\varphi}_i$ corresponding to an angle ϕ_i with respect to the horizontal direction. The control beam goes through a mask with two polarizers in the horizontal ($\vec{H}$) and vertical ($\vec{V}$) directions placed in front of the two pinholes L_c and R_c, respectively. The target beam passes through two pinholes L_t and R_t. A half-wave plate HWP$_{R_t}$, interchanging the H with the V polarization components, is placed in front of R_t. The double-pinhole at the control arm and the double-pinhole at the target arm of the interferometer are spatially "overlapped", i.e., L_c (R_c) and L_t (R_t) have equal longitudinal-transverse positions with respect to the correspondent optical axis. However, at each arm, the two pinholes are separated beyond the coherence length of the thermal field. The two light beams are then detected at the single-photon level by the two detectors D_c and D_t after passing

[1]University of Maryland Baltimore County, Department of Physics, Baltimore, Maryland 21250, USA. [2]Universität Ulm, Institut für Quantenphysik and Center for Integrated Quantum Science and Technology (IQST), Ulm, D-89069, Germany. Correspondence and requests for materials should be addressed to T.P. (email: taop1@umbc.edu) or V.T. (email: vincenzo.tamma@uni-ulm.de)
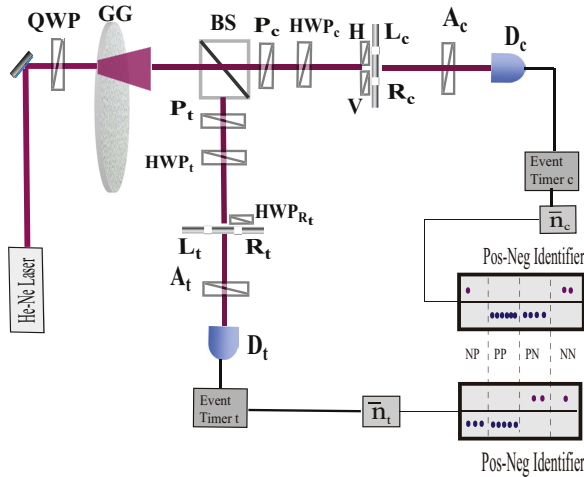
Figure 1. Schematic setup for the CNOT gate experimental simulation. The light emitted by a He-Ne laser is set to be left-circularly polarized. A rotating ground glass (*GG*) is then used to "thermalize" the coherent laser light into a large number of incoherent subfields. A beamsplitter (BS) splits the wavepackets into two beams. Polarizers P_i and half-wave plates HWP$_i$ ($i = c,t$) are used to prepare the "control" and "target" beams at polarization angles ϕ_c and ϕ_t, respectively, with respect to the horizontal direction. Each beam interacts with a mask with two pinholes L_i and R_i separated beyond the spatial coherence length of the thermal field. Two polarizers oriented in horizontal ($\vec{H}$) and vertical ($\vec{V}$) directions, respectively, are placed in front of pinholes L_c and R_c. A half-wave plate HWP$_{R_t}$, implementing a flip from H to V polarization and vice versa, is placed in front of the pinhole R_t. A_c–D_c and A_t–D_t are two independent polarizer-detectors performing single-photon detections at arbitrary polarization angles θ_i. A photon-number fluctuation correlation (PNFC) circuit is used to measure the photon-number fluctuation correlations between detectors D_c and D_t.

through the polarizers A_c and A_t, respectively. We consider a number $N \sim 4 \times 10^5$ of consecutive detection time intervals with width $\Delta t = 800 \ \mu s$. The value of Δt is small compared with the coherence time of the source, but large enough to guarantee enough counts per window. The registration times and the number $n_{ij}(\phi_i, \theta_i)$ of photo-detection events at each detector D_i within the jth time window, with $j = 1, \ldots, N$, are recorded for given output polarization angles θ_i by two independent but synchronized event timers. At each detector D_i the mean photon number $\bar{n}_i(\phi_i, \theta_i) \doteq \frac{1}{N}\sum_{j=1}^{N} n_{ij}(\phi_i, \theta_i)$ is obtained by averaging over all the values of photon number $n_{ij}(\phi_i, \theta_i)$ recorded in each of the N time windows j. The photon number fluctuation for each time window is calculated as[28]

$$\Delta n_{ij}(\phi_i, \ \theta_i) \doteq n_{ij}(\phi_i, \ \theta_i) - \bar{n}_i(\phi_i, \ \theta_i).$$

Finally, for given input polarization angles ϕ_c and ϕ_t of the control and target beams, respectively, the correlation

$$\langle \Delta n_c(\phi_c, \ \theta_c) \Delta n_t(\phi_t, \ \theta_t) \rangle = \frac{1}{N}\sum_{j=1}^{N} \Delta n_{cj}(\phi_c, \ \theta_c) \Delta n_{tj}(\phi_t, \ \theta_t) \tag{1}$$

in the photon-number fluctuations is measured at the output for arbitrary polarization angles θ_c and θ_t.

Interference between pairs of correlated paths and CNOT-gate simulation.

We consider first the case of input and output polarizations either in the horizontal direction $\vec{H}$ or in the vertical directions $\vec{V}$. In this case, the experimental outcomes in Fig. 2 for the correlation in the photon number fluctuations in Eq. (1) simulate the truth table (Table 1) of a CNOT-gate. The initial polarization direction $\vec{\phi}_c = \vec{H}, \ \vec{V}$ of the control beam remains always unchanged at the output. In particular, if the control beam is H-polarized then it can pass only through the pinhole L_c and a non-zero correlation in Eq. (1) is measured only when the target beam passes through the pinhole L_t without changing its initial polarization. On the other hand, a V-polarized control beam can only propagate through the pinhole R_c and a nontrivial correlation at the output occurs only if the target beam, by taking the path R_t, flips its polarization direction from $\vec{H}$ to $\vec{V}$ or vice versa. These experimental results witness the emergence of two pairs of correlated paths corresponding to the propagation through either the pinhole pair (L_c, L_t) or the pair (R_c, R_t). Can these pairs of correlated paths actually interfere? One may think that this is not possible since the two pinhole pairs are placed with respect to each other beyond the source coherence length. Interestingly, we show here experimentally that interference not only occurs but allows also us to fully simulate the entanglement operation of a CNOT gate. For this purpose, we consider the case where the control beam is polarized at an angle $\phi_c = \pi/4$ corresponding to the direction $\vec{\phi}_c = (\vec{H} + \vec{V})/\sqrt{2}$. In this case, by considering a target beam in the initial polarization direction $\vec{V}$, the correlation of the photon-number fluctuations in Fig. 3 measured at the interferometer output is given by
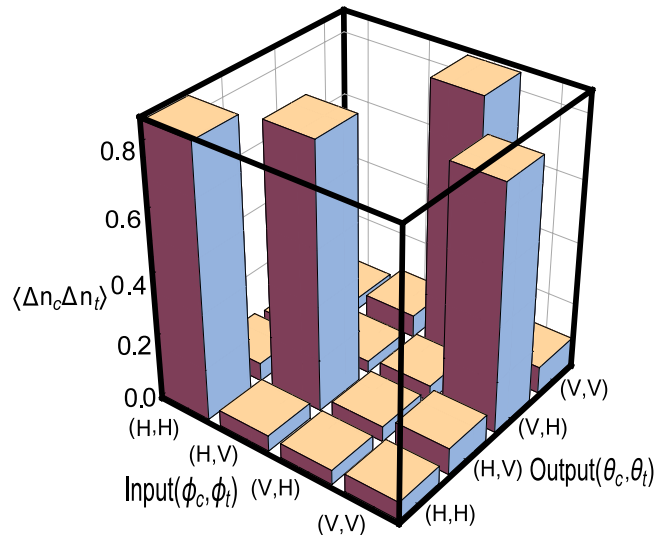
Figure 2. Experimental observation of the polarization correlation $\langle \Delta n_c(\phi_c, \theta_c) \Delta n_t(\phi_t, \theta_t) \rangle$ in the photon-number fluctuations for the input polarizations $(\phi_c, \phi_t) = (H, H), (H, V), (V, H), (V, V)$ and the output polarizations $(\theta_c, \theta_t) = (H, H), (H, V), (V, H), (V, V)$. For each input polarization (ϕ_c, ϕ_t), the plotted data are normalized by $\mathcal{N}(\phi_c, \phi_t) = \sum_{\theta_c, \theta_t} \langle \Delta n(\phi_c, \theta_c) \Delta n(\phi_t, \theta_t) \rangle$.

Input state	Output state			
	HH	**HV**	**VH**	**VV**
HH	1	0	0	0
HV	0	1	0	0
VH	0	0	0	1
VV	0	0	1	0

Table 1. Truth table for a CNOT gate operation.
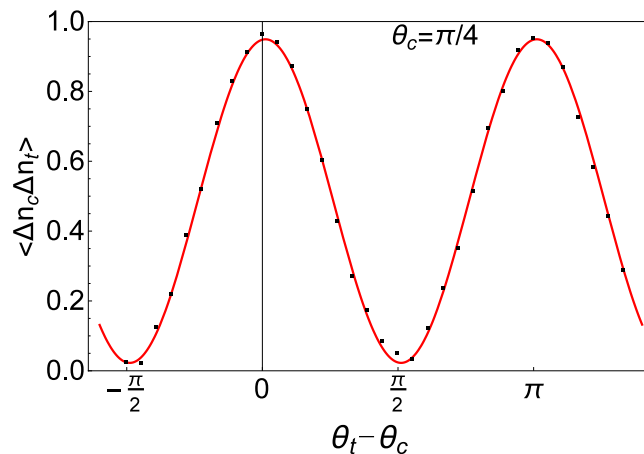
Figure 3. Experimental observation of the polarization correlation $\langle \Delta n_c(\phi_c, \theta_c) \Delta n_t(\phi_t, \theta_t) \rangle$ in the photon-number fluctuations for the input polarizations $\phi_c = \pi/4$ and $\phi_t = 0$. The black dots are experimental data normalized by $\langle n_c(\phi_c, \theta_c) \rangle \langle n_t(\phi_t, \theta_t) \rangle$, and the continuous red sinusoidal curve is a theoretical fitting based on Eq. (2). In this measurement, θ_c was fixed at $\pi/4$ and the values of θ_t range from $-\pi/4$ to $7\pi/4$.

$$\langle \Delta n_c(\phi_c, \theta_c) \Delta n_t(\phi_t, \theta_t) \rangle \propto \cos^2(\theta_t - \theta_c). \qquad (2)$$

Indeed, the measurement simulates with ~100% visibility the polarization correlations typical of the Bell state $|\Phi^+\rangle = (|HH\rangle + |VV\rangle)/\sqrt{2}$ produced at the output of a "genuine" CNOT gate with input state $|\phi_c\rangle|\phi_t\rangle$, where $|\phi_c\rangle = (|H\rangle + |V\rangle)/\sqrt{2}$ and $|\phi_t\rangle = |V\rangle$. Interestingly, entanglement correlations analogous to a CNOT operation

are simulated here by using only a separable input state and taking advantage of the interference between two pairs (L_c, L_t) and (R_c, R_t) of correlated paths, as will become more evident in the theoretical description in the next section.

Theoretical description. Here we provide a theoretical analysis based on the Glauber-Scully theory[39,40] of the experimental results described in the previous section. We start from modeling the state of the pseudo-thermal field. The ground glass contains a large number of tiny randomly shaped scattering diffusers, roughly a few micrometers in size. A large number of subfields or wave packets are scattered from the laser beam with random phases by these tiny diffusers. We consider each scattering diffuser as a sub-source. By considering, for simplicity, monochromatic light, the state of the pseudo-thermal field can be expressed in the coherent state representation as[41]

$$|\Psi\rangle \doteq \prod_{m,\mathbf{k}} |\alpha_m(\mathbf{k})\rangle,$$

where $\mathbf{k}$ is the transverse wavevector. $|\alpha_m(\mathbf{k})\rangle$ is an eigenstate of the annihilation operator $\hat{a}_m(\mathbf{k})$ with an eigenvalue $\alpha_m(\mathbf{k})$ which contains a real-positive amplitude $a_m(\mathbf{k})$ and a random phase $\varphi_m(\mathbf{k})$ arising from the scattering process associated with the mth diffuser.

We can then evaluate, for given input polarization angles ϕ_c and ϕ_t, the photon-number correlation

$$\langle n_c(\phi_c, \theta_c) n_t(\phi_t, \theta_t)\rangle \propto \langle\langle\Psi|\widehat{E}^{(-)}(\vec{r}_c, \phi_c, \theta_c)\widehat{E}^{(-)}(\vec{r}_t, \phi_t, \theta_t)\widehat{E}^{(+)}(\vec{r}_t, \phi_t, \theta_t)\widehat{E}^{(+)}(\vec{r}_c, \phi_c, \theta_c)|\Psi\rangle\rangle_{Es}, \quad (3)$$

where $\langle\ldots\rangle_{Es}$ denotes the ensemble average over all the possible values of $\alpha_m(\mathbf{k})$. Here, the field operator can be expressed as the sum

$$\widehat{E}^{(+)}(\vec{r}_i, \phi_i, \theta_i) = \sum_m \widehat{E}^{(+)}_{m,i}(\vec{r}_i, \phi_i, \theta_i) = \sum_m f_{m,i}(\mathbf{k}_m, \vec{r}_i, \phi_i, \theta_i)\hat{a}_m(\mathbf{k}_m),$$

with $i = c, t$, where $f_{m,i}(\mathbf{k}_m, \vec{r}_i, \phi_i, \theta_i)$ is an effective spatial transfer function (to be defined later) which takes into account the polarization dependent evolution from the mth pointlike diffuser to the pointlike detector D_i at position $\vec{r}_i$.

By introducing the "effective wavefunction"

$$\Psi_{m,i}(\vec{r}_i, \phi_i, \theta_i) \doteq \langle\alpha_m(\mathbf{k}_m)|\hat{E}^{(+)}_m(\vec{r}_i, \phi_i, \theta_i)|\alpha_m(\mathbf{k}_m)\rangle = f_{m,i}(\mathbf{k}_m, \vec{r}_i, \phi_i, \theta_i)\alpha_m(\mathbf{k}) \quad (4)$$

Eq. (3) becomes

$$\begin{aligned}\langle n_c(\phi_c, \theta_c) n_t(\phi_t, \theta_t)\rangle &= \langle n_c(\phi_c, \theta_c)\rangle\langle n_t(\phi_t, \theta_t)\rangle + \langle\Delta n_c(\phi_c, \theta_c)\Delta n_t(\phi_t, \theta_t)\rangle \\ &\propto \sum_m |\Psi_{m,c}|^2 \sum_n |\Psi_{n,t}|^2 + \sum_{m \neq n} \Psi^*_{m,c}\Psi_{m,t}\Psi^*_{n,t}\Psi_{n,c},\end{aligned}$$

leading to the correlation between the photon-number fluctuations:

$$\langle\Delta n_c(\phi_c, \theta_c)\Delta n_t(\phi_t, \theta_t)\rangle = \sum_{m \neq n} \Psi^*_{m,c}\Psi_{m,t}\Psi^*_{n,t}\Psi_{n,c} \propto \sum_m |\Psi^*_{m,c}\Psi_{m,t}|^2. \quad (5)$$

Here, the approximation in the second step of Eq. (5), given the large number of subfields, is used to simplify the notation.

We explicitly address the propagation through the two pinholes L_i and R_i at positions $\vec{r}_{L_i}$ and $\vec{r}_{R_i}$, respectively, at each interferometric arm in Fig. 1 by rewriting Eq. (4) as

$$\Psi_{m,i} = \Psi_{m,L_i} + \Psi_{m,R_i} = f_{m,L_i}(\mathbf{k}_m, \vec{r}_{L_i}, \vec{r}_i, \phi_i, \theta_i)\alpha_m(\mathbf{k}) + f_{m,R_i}(\mathbf{k}_m, \vec{r}_{R_i}, \vec{r}_i, \phi_i, \theta_i)\alpha_m(\mathbf{k}), \quad (6)$$

with

$$f_{m,L_c}(\mathbf{k}_m, \vec{r}_{L_c}, \vec{r}_c, \phi_c, \theta_c) \doteq \frac{1}{\sqrt{2}}(\vec{\phi}_c \cdot \vec{H})(\vec{H} \cdot \vec{\phi}_c) g_{m,L_c}(\mathbf{k}_m, \vec{r}_{L_c}, \vec{r}_c),$$

$$f_{m,R_c}(\mathbf{k}_m, \vec{r}_{R_c}, \vec{r}_c, \phi_c, \theta_c) \doteq \frac{1}{\sqrt{2}}(\vec{\phi}_c \cdot \vec{V})(\vec{V} \cdot \vec{\theta}_c) g_{m,R_c}(\mathbf{k}_m, \vec{r}_{R_c}, \vec{r}_c),$$

$$f_{m,L_t}(\mathbf{k}_m, \vec{r}_{L_t}, \vec{r}_t, \phi_t, \theta_t) \doteq \frac{i}{\sqrt{2}}(\vec{\phi}_t \cdot \vec{\theta}_t) g_{m,L_t}(\mathbf{k}_m, \vec{r}_{L_t}, \vec{r}_t),$$

$$f_{m,R_t}(\mathbf{k}_m, \vec{r}_{R_t}, \vec{r}_t, \phi_t, \theta_t) \doteq \frac{i}{\sqrt{2}}(\vec{\phi}^{(F)}_t \cdot \vec{\theta}_t) g_{m,R_t}(\mathbf{k}_m, \vec{r}_{R_t}, \vec{r}_t),$$

where g_{m,P_i} is the Green's function associated with the spatial propagation from the mth subfield to the detector D_i passing through the pinhole P_i ($P = L, R$), and "F" indicates the flip in the polarization components ($\vec{H}$ to $\vec{V}$ and vice versa) of the polarization direction $\vec{\phi}_t$ performed by the waveplate HWP$_{R_t}$.

By substituting Eq. (6) in Eq. (5) we obtain

$$\langle \Delta n_c(\phi_c, \theta_c) \Delta n_t(\phi_t, \theta_t) \rangle \propto \sum_m | \sum_{P=L,R} \Psi^*_{m,P_c} \Psi_{m,P_t} |^2 \propto \sum_m | \sum_{P=L,R} f^*_{m,P_c} f_{m,P_t} |^2,$$ (7)

where, in the second step of Eq. (7), the value $|\alpha_m(\mathbf{k})|^2$ was assumed to be the same for each subfield m.

Since the pinholes L_i and R_i are placed with respect to each other beyond the transverse coherence length of the thermal field, Eq. (7) reduces to[24]

$$\langle \Delta n_c(\phi_c, \theta_c) \Delta n_t(\phi_t, \theta_t) \rangle \propto \left| G_{L_c,L_t}(\theta_c, \theta_t) + G_{R_c,R_t}(\theta_c, \theta_t) \right|^2,$$ (8)

with

$$G_{P_c,P_t}(\theta_c, \theta_t) \doteq \sum_m f^*_{m,P_c} f_{m,P_t}.$$

Interestingly, the measured correlation in the photon-number fluctuations emerges from the interference between only two multiphoton contributions G_{L_c,L_t} and G_{R_c,R_t} associated with the propagation through the two pairs of pinholes (L_c, L_t) and (R_c, R_t), respectively.

We recall now that in the experiment, the two detectors are placed along the optical axes in the control and target arms of the interferometer and the two pinholes in each arm are at the same distances from the axes. In these conditions Eq. (8) becomes[24]

$$\langle \Delta n_c(\phi_c, \theta_c) \Delta n_t(\phi_c, \theta_t) \rangle \propto | \cos\phi_c \, \cos\theta_c \cos(\phi_t - \theta_t) + \, \sin\phi_c \sin\theta_c \sin(\phi_t + \theta_t) |^2.$$ (9)

We now compare this result with a genuine CNOT entangling operation on the input state $|\phi_c\rangle |\phi_t\rangle$, where $|\phi_c\rangle \doteq \cos\phi_c |H\rangle + \sin\phi_c |V\rangle$ and $|\phi_t\rangle \doteq \cos\phi_t |H\rangle + \sin\phi_t |V\rangle$, leading to the output entangled state

$$|\psi_{c,t}\rangle \doteq \cos\phi_c |H\rangle_c |\phi_t\rangle + \sin\phi_c |V\rangle |\phi_t^{(F)}\rangle,$$

where $|\phi_t^{(F)}\rangle \doteq \sin\phi_t |H\rangle + \cos\phi_t |V\rangle$. Polarization correlation measurements over the state $|\psi_{c,t}\rangle$ occur with a probability

$$P_{CNOT} \doteq |\langle \theta_c, \theta_t | \psi_{c,t} \rangle|^2 = | \cos\phi_c \cos\theta_c \cos(\phi_t - \theta_t) + \, \sin\phi_c \sin\theta_c \sin(\phi_t + \theta_t) |^2.$$ (10)

Comparing Eq. (10) with Eq. (9), it is clear that the measurement of correlations between the photon-number fluctuations at the two output ports leads to the simulation of a CNOT gate operation.

Discussion

In summary, we have experimentally demonstrated for the first time thermal light interference between two pairs of correlated paths, where each path in a pair is spatially incoherent with the paths in the other pair. This counterintuitive effect is at the very heart of the experimental simulation of a CNOT gate operation described here.

In particular, the simulation of the entanglement correlations typical of a CNOT-gate operation emerges from the interference between the two pairs of paths (L_c, L_t) and (R_c, R_t) in Fig. 1 propagating through two corresponding pairs of pinholes when correlation measurements in the photon-number fluctuations are performed at the output. Interestingly, this interference phenomenon occurs even if the pinholes in one pair are separated by more than the source coherence length with respect to the pinholes in the other pair.

Furthermore, the correlation in the photon-number fluctuations between the polarizations measured by the two distant detectors resembles the typical nonlocal behavior of entangled states even if no entanglement process occurs in the interferometer. Indeed, by not relying on complex non classical interferometers, the interference operation demonstrated here is apparently insensitive to photon losses and decoherence.

Lastly, by taking advantage of the abundant source of input states characterizing a thermal source with respect to single photon sources, this phenomenon can be used, in principle, to simulate correlations between a larger number of qubits, with potential applications in novel optical algorithms[8,42–46], imaging and metrology[8,18,24].

References

1. Brown, R. H. & Twiss, R. Correlation between photons in two coherent beams of light. *Nature* **177,** 27–29 (1956).
2. Brown, R. H. & Twiss, R. A test of a new type of stellar interferometer on sirius. *Nature* **178,** 1046–1048 (1956).
3. Alley, C. & Shih, Y. Foundations of quantum mechanics in the light of new technology, edited by m. namiki et all. *Physical society of Japan, Tokyo* **47** (1986).
4. Shih, Y. & Alley, C. O. New type of einstein-podolsky-rosen-bohm experiment using pairs of light quanta produced by optical parametric down conversion. *Physical Review Letters* **61,** 2921 (1988).
5. Hong, C., Ou, Z. & Mandel, L. Measurement of subpicosecond time intervals between two photons by interference. *Physical Review Letters* **59,** 2044 (1987).
6. Tamma, V. & Laibacher, S. Multiboson correlation interferometry with multimode thermal sources. *Physical Review A* **90,** 063836 (2014).
7. Tamma, V. & Laibacher, S. Multiboson correlation interferometry with arbitrary single-photon pure states. *Physical review letters* **114,** 243601 (2015).
8. Tamma, V. & Seiler, J. Multipath correlation interference and controlled-not gate simulation with a thermal source. *New Journal of Physics* **18,** 032002 (2016).
9. Nielsen, M. A. & Chuang, I. L. *Quantum computation and quantum information* (Cambridge university press, 2010).
10. Aaronson, S. & Arkhipov, A. The computational complexity of linear optics. In *Proceedings of the forty-third annual ACM symposium on Theory of computing*, 333–342 (ACM, 2011).

11. Laibacher, S. & Tamma, V. From the physics to the computational complexity of multiboson correlation interference. *Physical review letters* **115,** 243605 (2015).
12. Tamma, V. Sampling of bosonic qubits. *International Journal of Quantum Information* **12,** 1560017 (2014).
13. Tamma, V. & Laibacher, S. Boson sampling with non-identical single photons. *Journal of Modern Optics* **63,** 41–45 (2016).
14. Boto, A. N. *et al.* Quantum interferometric optical lithography: exploiting entanglement to beat the diffraction limit. *Physical Review Letters* **85,** 2733 (2000).
15. D'Angelo, M., Garuccio, A. & Tamma, V. Toward real maximally path-entangled n-photon-state sources. *Physical Review A* **77,** 063826 (2008).
16. Pittman, T., Shih, Y., Strekalov, D. & Sergienko, A. Optical imaging by means of two-photon quantum entanglement. *Physical Review A* **52,** R3429 (1995).
17. Gatti, A., Brambilla, E., Bache, M. & Lugiato, L. Correlated imaging, quantum and classical. *Physical Review A* **70,** 013802 (2004).
18. Valencia, A., Scarcelli, G., D'Angelo, M. & Shih & Y. Two-photon imaging with thermal light. *Physical review letters* **94,** 063601 (2005).
19. Lee, K. & Thomas, J. Experimental simulation of two-particle quantum entanglement using classical fields. *Physical review letters* **88,** 097902 (2002).
20. Fu, J., Si, Z., Tang, S. & Deng, J. Classical simulation of quantum entanglement using optical transverse modes in multimode waveguides. *Physical Review A* **70,** 042313 (2004).
21. Kagalwala, K. H., Di Giuseppe, G., Abouraddy, A. F. & Saleh, B. E. Bell's measure in classical optical coherence. *Nature Photonics* **7,** 72–78 (2013).
22. Qian, X.-F., Little, B., Howell, J. C. & Eberly, J. Shifting the quantum-classical boundary: theory and experiment for statistically classical optical fields. *Optica* **2,** 611–615 (2015).
23. Peng, T. & Shih, Y. Bell correlation of thermal fields in photon-number fluctuations. *EPL (Europhysics Letters)* **112,** 60006 (2016).
24. Cassano, M. *et al.* Spatial interference between pairs of optical paths with a chaotic source. *arXiv:1601.05045* (2016).
25. Knill, E., Laflamme, R. & Milburn, G. J. A scheme for efficient quantum computation with linear optics. *Nature* **409,** 46 (2001).
26. Duan, L. M. & Kimble, H. J. Scalable photonic quantum computation through cavity-assisted interactions. *Physical review letters* **92,** 127902 (2004).
27. Wei, H. R. & Deng, F. G. Scalable photonic quantum computing assisted by quantum-dot spin in double-sided optical microcavity. *Optics express* **21,** 17671–17685 (2013).
28. Chen, H., Peng, T. & Shih, Y. 100% correlation of chaotic thermal light. *Physical Review A* **88,** 023808 (2013).
29. Peng, T., Chen, H., Shih, Y. & Scully, M. O. Delayed-choice quantum eraser with thermal light. *Physical review letters* **112,** 180401 (2014).
30. Peng, T., Simon, J., Chen, H., French, R. & Shih, Y. Popper's experiment with randomly paired photons in thermal state. *EPL (Europhysics Letters)* **109,** 14003 (2015).
31. Martienssen, W. & Spiller, E. Coherence and fluctuations in light beams. *American Journal of Physics* **32,** 919–926 (1964).
32. Arecchi, F., Gatti, E. & Sona, A. Time distribution of photons from coherent and gaussian sources. *Physics Letters* **20,** 27–29 (1966).
33. Pittman, T., Jacobs, B. C. & Franson, J. Probabilistic quantum logic operations using polarizing beam splitters. *Physical Review A* **64,** 062311 (2001).
34. Pittman, T., Fitch, M., Jacobs, B. & Franson, J. Experimental controlled-not logic gate for single photons in the coincidence basis. *Physical Review A* **68,** 032316 (2003).
35. O'Brien, J. L., Pryde, G. J., White, A. G., Ralph, T. C. & Branning, D. Demonstration of an all-optical quantum controlled-not gate. *Nature* **426,** 264–267 (2003).
36. Gasparoni, S., Pan, J.-W., Walther, P., Rudolph, T. & Zeilinger, A. Realization of a photonic controlled-not gate sufficient for quantum computation. *Physical review letters* **93,** 020504 (2004).
37. Okamoto, R., Hofmann, H. F., Takeuchi, S. & Sasaki, K. Demonstration of an optical quantum controlled-not gate without path interference. *Physical review letters* **95,** 210506 (2005).
38. Bao, X. H., Chen, T. Y., Zhang, Q., Yang, J., Zhang, H., Yang, T. & Pan, J. W. Optical nondestructive controlled-NOT gate without using entangled photons. *Physical review letters* **98,** 170502 (2007).
39. Glauber, R. J. The quantum theory of optical coherence. *Physical Review* **130,** 2529 (1963).
40. Scully, M. O. & Zubairy, M. S. *Quantum optics* (Cambridge university press, 1997).
41. Shih, Y. *An introduction to quantum optics* (CRC press, 2011).
42. Tamma, V., Zhang, H., He, X., Garuccio, A. & Shih, Y. New factorization algorithm based on a continuous representation of truncated gauss sums. *Journal of Modern Optics* **56,** 2125–2132 (2009).
43. Tamma, V. *et al.* Factoring numbers with a single interferogram. *Physical Review A* **83,** 020304 (2011).
44. Tamma, V. Alley, C., Schleich, W. & Shih, Y. Prime number decomposition, the hyperbolic function and multi-path michelson interferometers. *Foundations of Physics* **42,** 111–121 (2012).
45. Tamma, V. *et al.* Analogue algorithm for parallel factorization of an exponential number of large integers: I. theoretical description. *Quantum Information Processing* 1–22 (2015).
46. Tamma, V. *et al.* Analogue algorithm for parallel factorization of an exponential number of large integers: II. optical implementation. *Quantum Information Processing* 1–15 (2015).

Acknowledgements

Author Contributions

T.P. constructed and performed the experiment. V.T. and Y.H.S. conceived the original idea. T.P. and Y.H.S. designed the experiment. T. P. analyzed the results. T. P., V.T. and Y.H.S. wrote the paper. All authors reviewed the manuscript.

Additional Information

Competing financial interests: The authors declare no competing financial interests.

How to cite this article: Peng, T. *et al.* Experimental controlled-NOT gate simulation with thermal light. *Sci. Rep.* **6**, 30152; doi: 10.1038/srep30152 (2016).